Carbon Support Effects on Bimetallic Pt−Ru Nanoparticles Formed from Molecular Precursors

Charles W. Hills, Michael S. Nashner, Anatoly I. Frenkel, John R. Shapley,* and Ralph G. Nuzzo*

School of Chemical Sciences and the Frederick Seitz Materials Research Laboratory, University of Illinois, Urbana, Illinois 61801

Received July 21, 1998. In Final Form: December 2, 1998

We describe the preparation, structural characterization, and support interactions experienced by two different compositions of Pt−Ru nanoparticles supported on several carbons (carbon black, fullerene soot, and desulfurized carbon black). The bimetallic nanoparticles, obtained by reduction of the neutral molecular precursors $PtRu_5C(CO)_{16}$ and $Pt_2Ru_4(CO)_{18}$ (the latter of which lacks a central "stabilizing" carbide core) at elevated temperatures in a hydrogen atmosphere, show a structural homology, exhibiting exceptionally narrow size and compositional distributions. A detailed structural picture of the nanoparticles has been deduced on the basis of in-situ extended X-ray absorption fine structure (EXAFS), scanning transmission electron microscopy (STEM), energy-dispersive X-ray analysis (EDX), and X-ray absorption near edge structure (XANES). These techniques reveal that the bimetallic nanoparticles have Pt/Ru compositions of 1:5 and 2:4, respectively, and average diameters lying between 1.0 and 1.5 nm. The local metal coordination environments reveal a nonstatistical distribution of the two metals in the nanoparticles. Specifically, Pt shows a marked preference for segregation to the particle surfaces under an H_2 atmosphere. The data also reveal a difference in the structural environment of the nanoparticles when formed on the fullerene soot support. Interactions between Ru and low-*Z* atoms are revealed through XANES, which, taken collectively with the other data presented, leads us to propose a possible Ru−C compound formation on this latter support phase.

Introduction

Nanometer-sized metal particles are of interest, in part due to their unique physical and chemical properties as well as their importance as catalysts.[1−6] The physical properties of nanoparticles, which depend strongly on the perturbations that arise from the large fraction of metal atoms residing at the particle surface, may show a marked difference from those characterizing the bulk solid state.[1−6] A significant motivation of current research is the need to develop a predictive understanding of the structure and reactivity of supported alloy (bimetallic) nanoparticles due to the profound improvements they yield in many industrial catalytic processes.[1,4,6] Despite the extensive efforts of research to date, such an understanding has yet to be obtained.

Multicomponent supported metal catalysts can be prepared by a number of synthetic methods, each with its own distinct advantages. The most commonly used coimpregnation methods involve a support material that has been modified by the adsorption of metal ion precursors from solution.[6,7] The condensation of these centers upon reduction (e.g., in flowing H_2 at high temperature) yields the desired bimetallic particle catalysts. The control of the particle size distribution obtained in this way is quite limited, and the nature of the compositional distributions that characterize the sample is often unknown. An attractive alternative to the coimpregnation method is the use of molecular cluster compounds as precursors.[6] We have previously shown that molecular clusters provide an advantageous means for preparing metal alloy catalysts, since the cluster predetermines the proper stoichiometry of the metal atoms.[6]

In the present report, we describe the synthesis of Pt−Ru alloy nanoclusters derived from molecular cluster precursors with two core compositions ($PtRu_5$ and Pt_2Ru_4). In bulk, these compositions straddle a stability limit in the binary phase diagram.[8] Solids with a $PtRu_5$ composition are hcp in structure (although nanometer-sized clusters of this composition adopt an fcc close-packed structure).[6a] A composition of Pt_2Ru_4, on the other hand, is expected to phase separate into coexistent hcp (Ru rich) and fcc alloys. This study also specifically investigates the role played by support effects (carbon in this case) in

(1) (a) Sinfelt, J. H.; Via, G. H.; Lytle, F. W. *J. Chem. Phys.* **1980**, *72*, 4832. (b) Via, G. H.; Drake, K. F.; Meitzner, G.; Lytle, F. W.; Sinfelt, J. H. *Catal. Lett.* **1990**, *5*, 25. (c) Liang, K. S.; Chien, F. Z.; Hughes, G. J.; Meitzner, G. D.; Sinfelt, J. H. *J. Phys. Chem.* **1991**, *95*, 9974. (d) Davis, R. J.; Boudart, M. *J. Phys. Chem.* **1994**, *98*, 5471. (e) Merlen, E.; Beccat, P.; Bertolini, J. C.; Delichère, P.; Zanier, N.; Didillon, B. *J. Catal.* **1996**, *159*, 178.

(2) (a) Malm, J.; Bovin, J.; Petford-Long, A.; Smith, D. J.; Schmid, G. *Angew. Chem., Int. Ed. Engl.* **1988**, *27*, 555. (b) Aleandri, L. E.; Bönnemann, H.; Jones, D. J.; Richter, J.; Rozière, J. *J. Mater. Chem.* **1995**, *5*, 749. (c) Bradley, J. S.; Via, G. H.; Bonnevoit, L.; Hill, E. W. *Chem. Mater.* **1996**, *8*, 1895. (d) Rodriquez, A.; Amiens, B.; Chaudret, P.; Casanove, M.-J.; Lacante, P.; Bradley, J. S. *Chem. Mater.* **1996**, *8*, 1978. (e) Kolb, U.; Quaiser, S. A.; Winter, M.; Reetz, M. T. *Chem. Mater.* **1996**, *8*, 1889.

(3) Nashner, M. S.; Somerville, D. M.; Lane, P. D.; Adler, D. L.; Shapley, J. R.; Nuzzo, R. G. *J. Am. Chem. Soc.* **1996**, *118*, 12964.

(4) (a) Iwasita, T.; Nart, F. C.; Vielstich, W. *Ber. Bunsen-Ges. Phys. Chem.* **1990**, *94*, 1030. (b) Leger, J. M.; Lamy, C. *Ber. Bunsen-Ges. Phys. Chem.* **1990**, *94*, 1021. (c) Ross, P. N. *Electrochim. Acta* **1991**, *36*, 2053. (d) Cameron, D. S.; Hards, G. A.; Thomsett, D. In *Proceedings of the Workshop on Direct Methanol-Air Fuel Cells*; Landgrebe, A. R., Sen, R. K., Wheeler, D. J., Eds.; Proceedings Series; The Electrochemical Society: Pennington, NJ, 1992; PV 92-14, pp 10−23.

(5) (a) McBreen, J.; Mukerjee, S. *J. Electrochem. Soc.* **1995**, *142*, 3399. (b) Chang, J.-R.; Lee, J.-F.; Lin, S. D.; Lin, A. S. *J. Chem. Phys.* **1995**, *99*, 14798.

(6) (a) Nashner, M. S.; Frenkel, A. I.; Adler, D. L.; Shapley, J. R.; Nuzzo, R. G. *J. Am. Chem. Soc.* **1997**, *119*, 7760 and all references therein. (b) Nashner, M. S.; Frenkel, A. I.; Somerville, D.; Hills, C. W.; Shapley, J. R.; Nuzzo, R. G. *J. Am. Chem. Soc.* **1998**, *120*, 8093.

(7) (a) Kinoshita, K.; Stonehart, P. In *Preparation and Characterization of Highly Dispersed Electrocatalytic Materials*; Kinoshita, K., Stonehart, P., Eds.; Plenum: New York, 1977; Vol. 12, pp 183−266. (b) Watanabe, M.; Uchida, M.; Motoo, S. *J. Electroanal. Chem.* **1987**, *229*, 395.

(8) Hutchinson, J. M. *Platinum Met. Rev.* **1972**, *16*, 88.

10.1021/la980921b CCC: $18.00
Published on Web 01/06/1999

mediating the transport-limited aggregation of the precursor clusters, which condense to form the final nanoparticles. Carbon-supported Pt−Ru particles have superior activity as anode catalysts for methanol electrooxidation and demonstrate a marked improvement in resistance to poisoning in comparison to unalloyed Pt.[4] These improvements are significant but have yet to relieve the need for more active electrocatalyst materials for commercially viable direct methanol fuel cells (DMFCs). Much of the current understanding of the mechanisms involved in methanol oxidation with Pt−Ru electrocatalysts is based either on studies of well-defined planar-polycrystalline Pt−Ru electrodes[9] or on the electrochemical polarization responses of model cell assemblies which contain fairly significant loadings of the metal-alloy catalysts.[4,5] A detailed understanding of the compositional and size dependencies of the electrocatalytic reaction rates over nanometer-sized supported bimetallic particles has yet to be obtained.

We report the synthesis and structural characterization of carbon-supported Pt−Ru nanoparticles prepared by using the neutral complexes $PtRu_5C(CO)_{16}$ and $Pt_2Ru_4(CO)_{18}$ as molecular cluster precursors. The structures of these precursors differ markedly[10] and thus serve to probe the sensitivity of the nanocluster synthesis to this aspect of the molecular design. Our results show that activation of the cluster precursors on a variety of supports leads to the formation of bimetallic particles showing a structural homology (i.e., clusters with narrow compositional and size distributions). The atomic-scale structures of the resulting particles, referred to hereafter as $[PtRu_5]$/C and $[Pt_2Ru_4]$/C, have been characterized with in-situ extended X-ray absorption fine structure (EXAFS) spectroscopy, scanning transmission electron microscopy (STEM), and X-ray absorption near edge structure (XANES). These experiments show that the supported bimetallic nanoparticles have Pt/Ru compositions of 1:5 and 2:4, respectively, and diameters between 1.0 and 1.5 nm. On the basis of a comparative analysis of the STEM and EXAFS data (which reveal the average nanoparticle size and metal coordination numbers, respectively), the nanoparticles are found to adopt a closest-packed, nonspherical structural motif. The local metal coordination environment shows the presence of a nonstatistical distribution of the different metal atoms in the nanoparticles. Specifically, we find that the Pt atoms in the particle show a pronounced tendency to self-segregate to surface sites on the bimetallic particles. The local bonding environments surrounding the Ru atoms, however, show a marked sensitivity to the chemical nature of the carbon support. For example, the Ru−C interactions seen on carbon black and a (so-called) fullerene soot are found to be very different. The consequences of these differences on the structural evolution of the nanoparticles and their electronic structure are explored.

Experimental Section

Sample Preparation. The molecular cluster precursors, $PtRu_5C(CO)_{16}$ and $Pt_2Ru_4(CO)_{18}$, were prepared by methods described in the literature.[10] The fullerene soot support materials (prepared by arc methods and which are depleted in C_{60} and C_{70} fullerenes) were obtained from SES Research, Inc. A suitable quantity of the compound (1−2 wt % metal loading) was dispersed on carbon black (Vulcan XC-72, Cabot), electrochemically desulfurized carbon black (Vulcan XC-72, Cabot),[11] or fullerene soot by incipient wetness from a THF solution. The mixture was allowed to dry in air for 0.5 h. The metallic particles were obtained by heating the supported molecular precursors in a H_2 atmosphere as described earlier.[6]

Scanning Transmission Electron Microscopy. Microscopy studies were performed using a field emission Vacuum Generators HB501 scanning transmission electron microscope operated at 100 kV. The specimens were prepared by dipping copper-mesh-supported holey carbon grids (SPI supplies) into powdered samples that had been previously activated and examined in situ by EXAFS. Image analysis was performed with Digital-micrograph (Gatan) digital-video data-acquisition software. The particle sizes were determined by measuring the cross-section intensity profiles of individual nanoparticles. The particle diameter was measured as the full width at half-maximum of the intensity profile.

The composition of the selected nanoparticles was determined by energy-dispersive X-ray (EDX) analysis.[12,13] In this analysis, the incident electron probe beam was located on a single particle and the X-ray fluorescence was detected. EDX data acquisition and analysis was performed using Link ISIS (Oxford) software, and the quantitative analyses were based on the characteristic X-ray fluorescence lines of Pt and Ru (Ru Lα,β, 2.6 keV; Ru Lγ, 3.2 keV; Ru Kα, 19.2 keV; Pt Mα,β, 2.1 keV; Pt Lα, 9.4 keV; Pt Lα, 11.1 keV; Pt Lβ, 11.3 keV). EDX data were also measured from a standard of known composition, prepared by dispersing the molecular precursors onto a holey carbon Cu grid from a THF solution. The grid was allowed to dry in air and was then placed in the microscope for analysis.

In-Situ Extended X-ray Absorption Fine Structure. To collect in-situ X-ray absorption data from the catalyst-containing sample, about 25 mg of the support, containing the molecular precursor, was pressed at a load of ∼5 tons into a rectangular wafer (ca. 1.5 × 1.0 cm) using a hydraulic pellet press. To avoid thickness effects (i.e., self-absorption),[14] the wafers formed had a thickness (d) of 0.5 mm, satisfying the condition that $\Delta\mu x = 0.1$, where x is the effective sample thickness (d/cos 45°) and $\Delta\mu$ is the absorbance at both the Pt L_3 and Ru K absorption edge steps. The wafer was then loaded into a custom-designed and -built catalyst cell which allowed simultaneous in-situ X-ray fluorescence and transmission measurements over the operating temperature range 150−773 K.

After the sample wafer was loaded, the in-situ cell was purged with H_2 for 1 h. To remove O_2 and water, the metered flow of H_2 (Matheson, 99.999%) was passed through sorbant traps (Alltech). The temperature was monitored with a chromel/alumel thermocouple (Omega) mounted directly on the sample-mounting stage. The sample activation was achieved by heating at a rate of 15 K/min in flowing H_2 (40 mL/min) to a temperature of 673 K, at which the sample was held for 1 h. During the activation, the XANES region of the Pt L_3 edge was scanned. The samples were then cooled in a H_2 atmosphere to 190 K before making the EXAFS measurements.

X-ray absorption data for the Pt L_3 and Ru K edges were also measured from the following reference compounds: Ru powder (Aldrich) and Pt foil (0.005 mm) (Aldrich). The Ru powder was alternately ground and sieved (200 mesh) to yield an average particle size of less than 10 μm, as ascertained with an optical microscope. The thickness effect in the EXAFS experiment was

(9) (a) Ross, P. N. In *Proceedings of the Workshop on Direct Methanol-Air Fuel Cells*; Landgrebe, A. R., Sen, R. K., Wheeler, D. J., Eds.; Proceedings Series; The Electrochemical Society: Pennington, NJ, 1992; PV 92-14, pp 51−69. (b) Gasteiger, H. A.; Markovic, N.; Ross, P. N.; Cairns, E. J. *J. Phys. Chem.* **1993**, *97*, 12020. (c) Gasteiger, H. A.; Markovic, N.; Ross, P. N.; Cairns, E. J. *J. Electrochem. Soc.* **1994**, *141*, 1795. (d) Gasteiger, H. A.; Markovic, N.; Ross, P. N.; Cairns, E. J. *J. Phys. Chem.* **1994**, *98*, 617. (e) Gasteiger, H. A.; Markovic, N. M.; Ross, P. N., Jr.; Cairns, E. J. *Electrochim. Acta* **1994**, *39*, 1825. (f) Gasteiger, H. A.; Markovic, N. M.; Ross, P. N. *J. Phys. Chem.* **1995**, *99*, 8290.

(10) (a) Adams, R. D.; Wu, W. *J. Cluster Sci.* **1991**, *2*, 271. (b) Adams, R. D.; Chen, G.; Wu, W. *J. Cluster Sci.* **1993**, *4*, 119.

(11) The desulfurized carbon black was a gracious gift from Dr. Debra Rolison at the Naval Research Laboratory.

(12) Gallezot, P.; Leclerq, C. In *Characterization of Catalysis by Conventional and Analytical Electron Microscopy*; Gallezot, P., Leclerq, C., Eds.; Plenum: New York, 1994; pp 509−558.

(13) Edington, J. W. *Practical Electron Microscopy*; Philips: Eindhoven, The Netherlands, 1975.

(14) Tan, Z.; Budnick, J. I.; Heald, S. M. *Rev. Sci. Instrum.* **1989**, *60*, 1021.

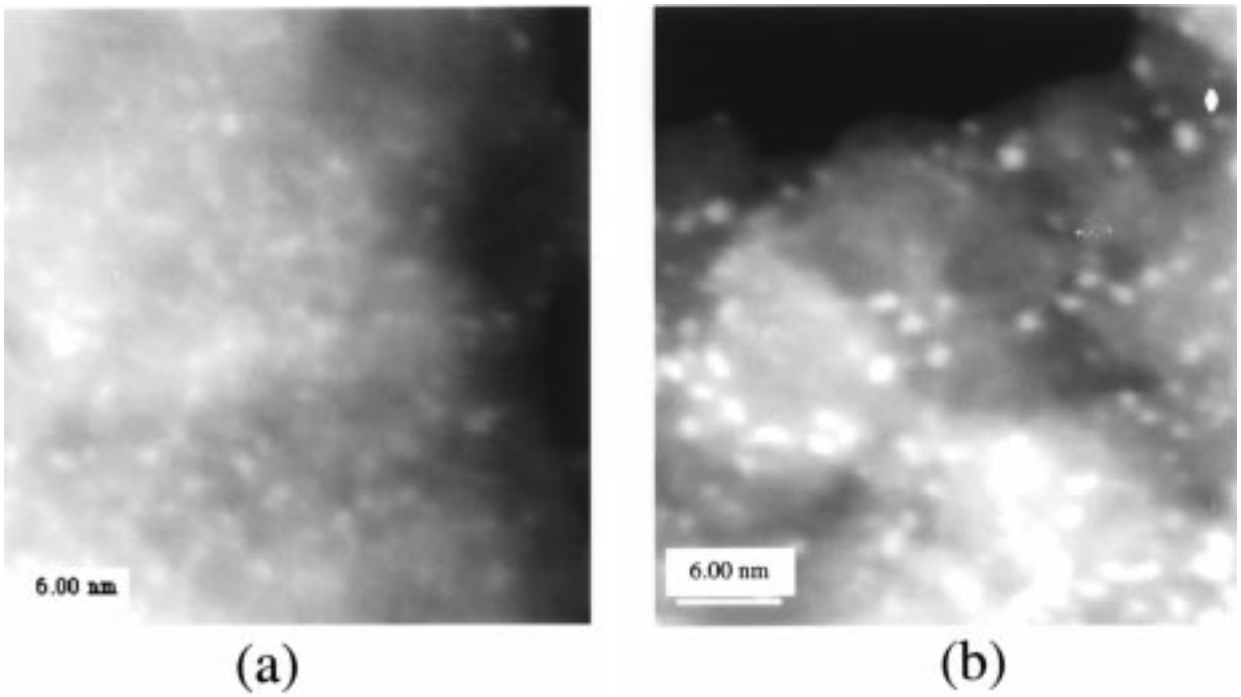

Figure 1. Representative STEM dark-field images ($\times 10^6$, 100 kV) of the carbon-supported [$PtRu_5$]/C nanoparticles: (a) [$PtRu_5$]/fullerene soot; (b) [$PtRu_5$]/desulfurized carbon black.

minimized by having the thickness x of the reference samples yield the optimum condition of the transmission EXAFS experiment: $\Delta\mu x \approx 1$. In our measurements, the edge jumps of the absorption coefficients were obtained to be 1.2 for the Pt L_3 edge and 0.84 for the Ru K edge. Therefore, the thickness effect can be neglected in both measurements.

All X-ray absorption data were measured at the National Synchrotron Light Source, located at the Brookhaven National Laboratory in Upton, New York. The UIUC/AT&T beamline X16C was used for all measurements. The X16C beamline uses a sagitally focusing monochromator with Si(111) crystals which focus 3.5 mrad of light into a 0.3 mm × 0.5 mm beam spot at the sample. The intensity of the focused beam (I_0) was measured with a 15 in. ion chamber filled with a 10:1 mixture of He/Ar for the Pt L_3 edge and with pure Ar for the Ru K edge measurements, respectively. X-ray absorption data from the samples were measured simultaneously in transmission and fluorescence modes by scanning from 200 eV below to 1000 eV above the Pt L_3 and Ru K edges. This was accomplished by turning the sample to ~45° with respect to the incident beam and measuring the intensity of the transmitted (I_1) X-rays and the intensity of the X-ray fluorescence (I_f). A 15 in. Ar-filled ion chamber placed after the sample (collinear with the beam direction) was used to measure I_1, and a Lytle detector (EXAFS Co.) placed at 90° with respect to the beam direction was used to measure I_f. Thin samples of Pt and Ru metal were used to calibrate the beam energy during each scan of the Pt L_3 and Ru K edges, respectively. The calibration measurement was made with a third ion chamber (I_2) placed after I_1. The positions of the metal absorption edges (Pt, 11564 eV; Ru, 22117 eV) could then be determined by placing the metal standard between the ion chambers I_1 and I_2 and measuring the absorption coefficient $\mu x = \ln(I_1/I_2)$ due to the metal standard.

EXAFS Data Analysis. The analytical procedures used follow that described in detail elsewhere.[6]

Results

The structures of the supported bimetallic nanoparticles, prepared by heating the carbon-supported $PtRu_5C(CO)_{16}$ and $Pt_2Ru_4(CO)_{18}$ compounds to 673 K in an H_2 atmosphere, were deduced using several independent methods.

Characterization of Nanoparticle Structure and Composition by Scanning Transmission Electron Microscopy. Representative dark-field images of the carbon-supported [$PtRu_5$]/C and [Pt_2Ru_4]/C samples are shown in Figures 1 and 2, respectively. The samples analyzed in the micrographs are the same as those prepared and characterized in the in-situ EXAFS experiment. The micrographs in Figure 1 correspond to $PtRu_5$ supported on a fullerene soot support (Figure 1a) and desulfurized carbon black (Figure 1b). The structure of clusters formed on a nascent carbon black support has been previously described.[6a] The clusters in Figure 2a correspond to Pt_2Ru_4 nanoparticles supported on a nascent carbon black support, while those in Figure 2b were prepared using a fullerene soot support. As indicated by the particle size histograms shown in Figures 3 and 4, the particles formed by the $PtRu_5$ and Pt_2Ru_4 precursors all have a comparable average diameter (between 1.0 and 1.5 nm), with little sensitivity to the nature of the support carbon used. Specifically, the [$PtRu_5$] supported on fullerene soot has an average particle diameter of approximately 1.0 nm, while the desulfurized carbon black shows an average diameter of approximately 1.1 nm. We have reported earlier that the average particle size for [$PtRu_5$] supported on carbon black is approximately 1.5 nm.[6a] For the [Pt_2Ru_4] supported on carbon black, we find an average particle size of 1.4 nm, whereas the nanoparticles supported on fullerene soot have an average diameter of approximately 1.1 nm. Particle formation for this cluster composition was not examined on the desulfurized carbon black support.

The composition of individual particles was probed using energy-dispersive X-ray analysis (EDX).[12,13] Quantitative analysis of the fluorescence yield revealed the composition of the particles. The reference molecular precursors $PtRu_5C(CO)_{16}$ and $Pt_2Ru_4(CO)_{18}$ were found to have an average Ru content of 86 ± 1 and 72 ± 1 atom %, respectively. These values compare well with the expected values based on the known stoichiometry of the complex and serve to calibrate the response of the detector (the few percent deviation is well within the error limits of the detector calibration). Table 1 shows the composition of

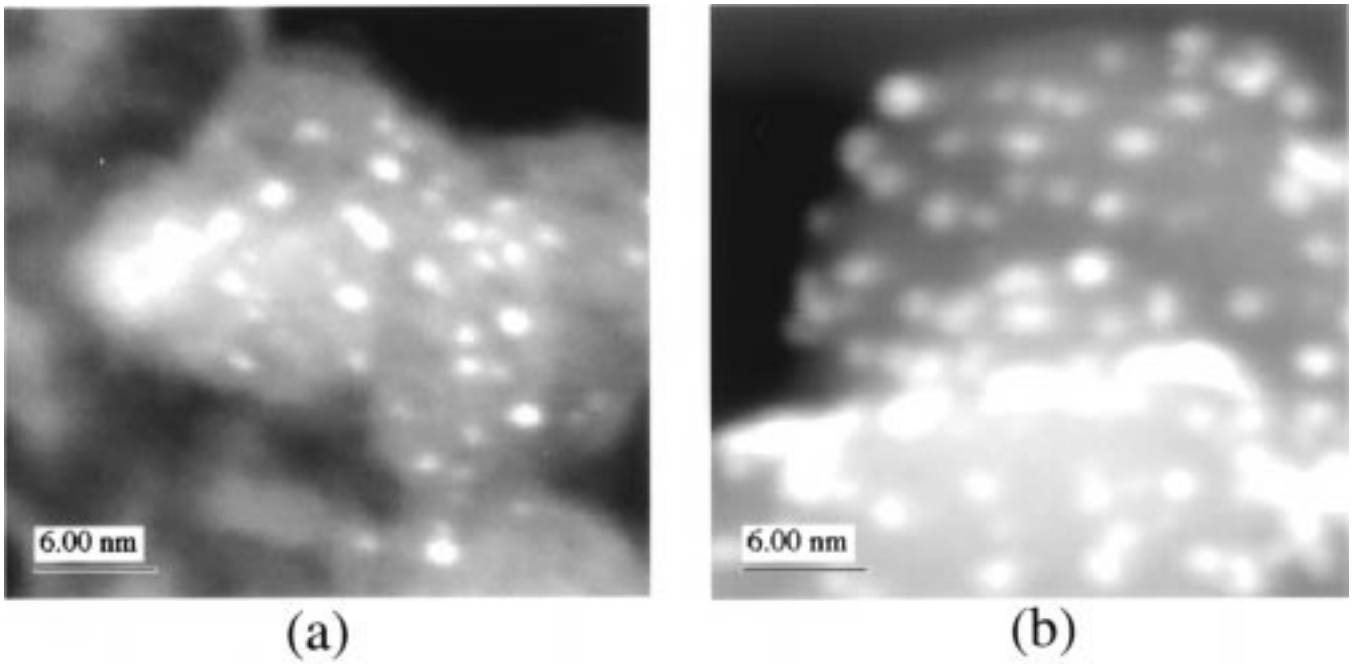

Figure 2. Representative STEM dark-field images ($\times 10^6$, 100 kV) of the carbon-supported $[Pt_2Ru_4]$/C nanoparticles: (a) $[Pt_2Ru_4]$/carbon black; (b) $[Pt_2Ru_4]$/fullerene soot.

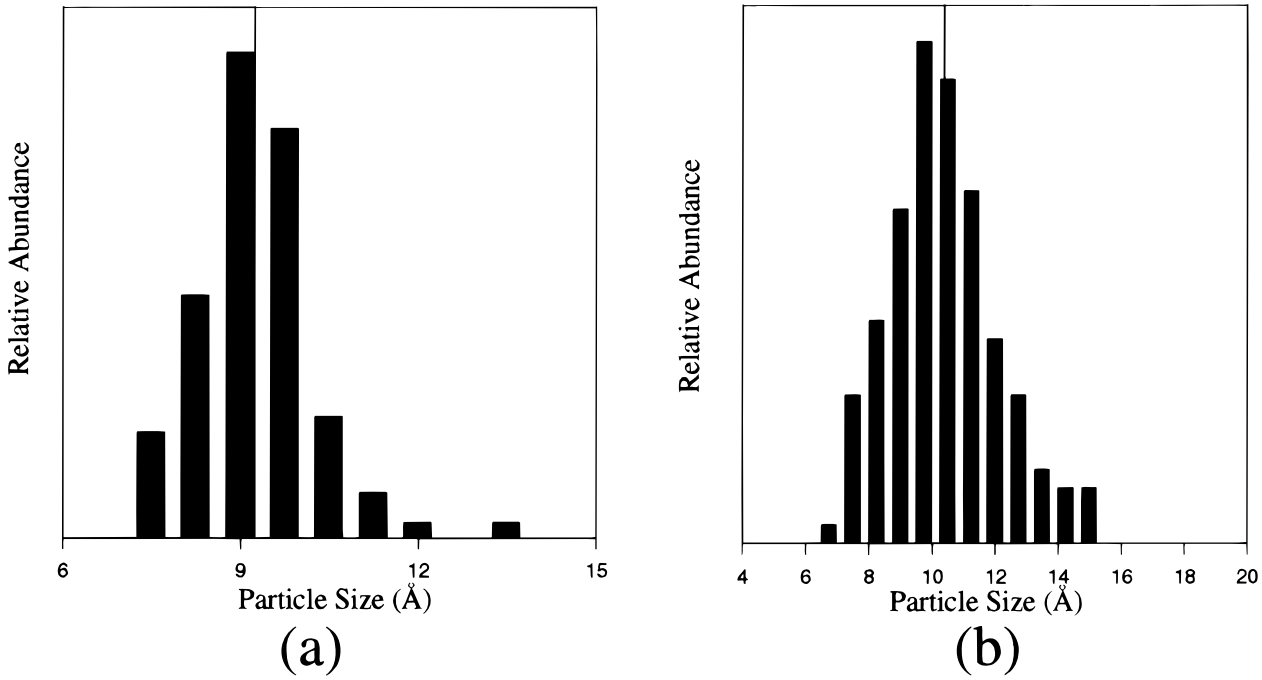

Figure 3. Histograms of the particle size distribution of the $[PtRu_5]$/C nanoparticles measured from multiple STEM images taken in different sample regions: (a) $[PtRu_5]$/fullerene soot; (b) $[PtRu_5]$/desulfurized carbon black.

the carbon-supported nanoparticles compared to the molecular precursors. Generally, the metal clusters' composition closely tracks that of the precursor with the measured values all lying within the range of the experimental uncertainty. The half widths at half-height of the distribution of the measured elemental contents (measured for >25 clusters) were of the order of plus or minus several percent. The results follow those of a more elaborate analysis previously reported for $[PtRu_5]$/C.[6a]

Binary Alloy Nanoparticle Structure Deduced from the Measurement of in-situ EXAFS. Figure 5 displays the background-subtracted k^2-weighted Pt L_3 edge spectra collected on Pt foil and the Ru K edge EXAFS data from Ru powder. The Pt L_3 and Ru K edge data for $[PtRu_5]$/C and $[Pt_2Ru_4]$/C are shown in Figures 6 and 7, respectively. The qualitative similarity between the functional forms of the EXAFS amplitudes measured from the reference materials and the supported nanoparticles suggests that the Pt and Ru centers are coordinated by predominantly metal scatterers.[15] The significant reduction in the scattering amplitude (Figures 6 and 7) seen over the entire k range, in comparison to the reference amplitude (Figure 5), is directly reflective of an enhanced

(15) (a) Stern, E. A.; Heald, S. M. In *Handbook on Synchotron Radiation*; Koch, E. E., Ed.; North-Holland: Amsterdam, 1983; Vol. 1, Chapter 10. (b) Koningsberger, D. C., Prins, R., Eds.; *X-ray Absorption: Principles, Applications, Techinques of EXAFS, SEXAFS, and XANES*; Wiley: New York, 1988.

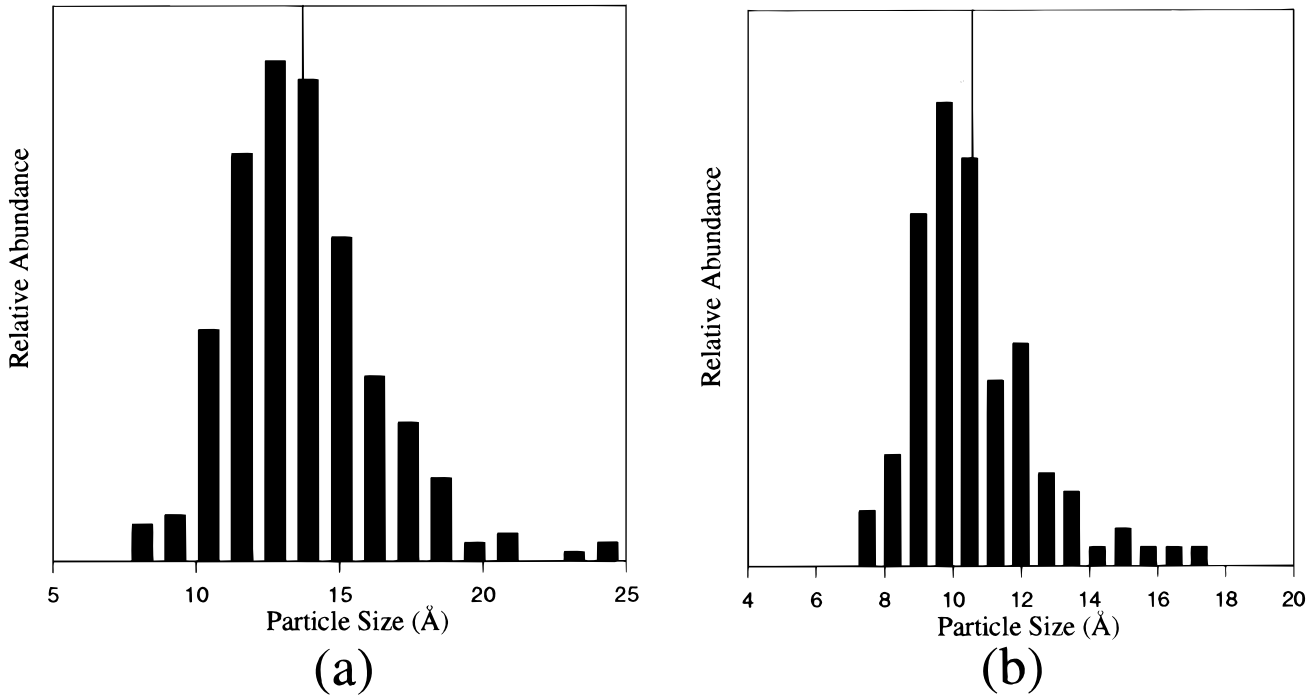

Figure 4. Histograms of the particle size distribution of the $[Pt_2Ru_4]$/C nanoparticles measured from multiple STEM images taken in different sample regions: (a) $[Pt_2Ru_4]$/carbon black; (b) $[Pt_2Ru_4]$/fullerene soot.

Table 1. Nanocluster Composition Obtained from Energy-Dispersive X-ray Analysis (EDX)

	Ru atom %	Pt atom %
$PtRu_5C(CO)_{16}$	85.9 ± 1.3	14.1 ± 1.3
$[PtRu_5]$/carbon black	85.7 ± 2.8	14.3 ± 2.8
$[PtRu_5]$/fullerene soot	84.5 ± 4.9	15.5 ± 4.9
$[PtRu_5]$/desulfurized carbon black	85.6 ± 2.7	14.4 ± 2.7
$Pt_2Ru_4(CO)_{18}$	71.8 ± 1.3	28.2 ± 1.3
$[Pt_2Ru_4]$/carbon black	75.1 ± 6.0	24.9 ± 6.0
$[Pt_2Ru_4]$/fullerene soot	67.1 ± 5.7	32.9 ± 5.7

disorder and/or lower average coordination number.[6] Figure 8 shows the magnitude of the Fourier transformed (FT) EXAFS of the Pt foil and the Ru powder, while Figures 9 and 10 show the FT EXAFS of the supported nanoparticles ($[PtRu_5]$/C and $[Pt_2Ru_4]$/C, respectively). These data yield the non-phase-corrected radial structure functions around Pt and Ru centers. As is shown below, the dominant peaks at approximately 2.5 Å in the FT data for $[PtRu_5]$ (Figure 9) and approximately 2.7 Å in the FT data for $[Pt_2Ru_4]$ (Figure 10) result from a combination of scattering from Pt and Ru atoms in the first shell (i.e., nearest neighbors). The data sets for the nanoparticles also show a significant higher-shell coordination (i.e., in the r range 3−5.6 Å) that is similar to that shown for the reference data. The Pt edge data, however, have distinctively larger signals in the higher shells than the Ru edge data, as was expected from past studies of $[PtRu_5]$/C.[6]

The EXAFS data fit for the nanoparticles was performed, assuming a closest-packed shell structure as was previously verified,[6] in order to extract the structural parameters for each metal absorber. Both backscatterers (Pt and Ru) had to be accounted for in the fits of the Pt and Ru EXAFS data. Therefore, all possible Pt−M(1) and Ru−M(1) paths (where M = Pt and Ru) from the first shell had to be accounted for in the theoretical fit of the Pt L_3 and Ru K edge EXAFS data. The nanoparticle was modeled using an fcc structure, and the number of heterometallic bonding interactions was fixed in accordance with the composition ratio, 1:5 for $[PtRu_5]$ and 2:4 for $[Pt_2Ru_4]$.

The Pt L_3 and Ru K edge data from the nanoparticles were fit simultaneously. The advantage of a simultaneous

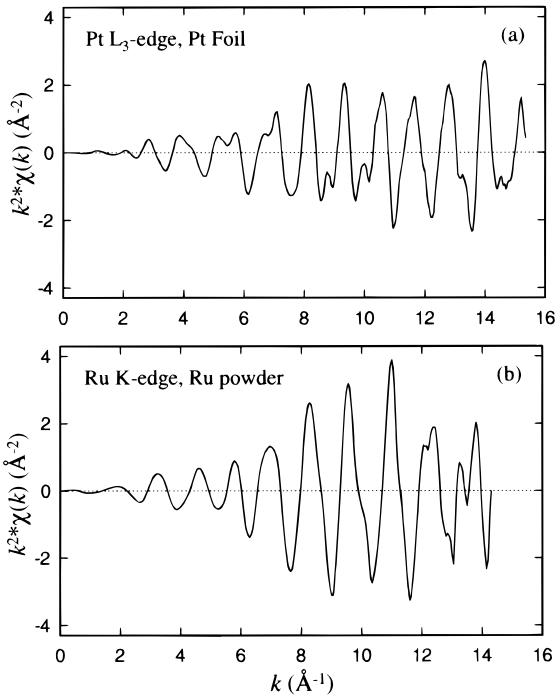

Figure 5. Raw $k^2\chi(k)$ (Å^{-2}) EXAFS data measured from the reference materials at 190 K: (a) the Pt L_3 edge from a Pt foil (0.005 mm); (b) the Ru K edge from Ru powder.

fit to the two edges of the same material is in decreasing the ratio between the number of fit variables and the number of independent points in the data. This is possible due to the fact that the structural parameters of the heterometallic bonds (i.e., Pt−Ru and Ru−Pt) must be the same, as seen from each edge, while the number of independent points doubles when adding a second data set. The fit was carried out by simultaneously fitting both edges over an r range of 2.0−3.1 Å for the dominant first-shell single scattering paths (i.e., Pt−Ru(1), Pt−Pt(1), Ru−Pt(1), Ru−Ru(1)). The results of the first-shell fits are

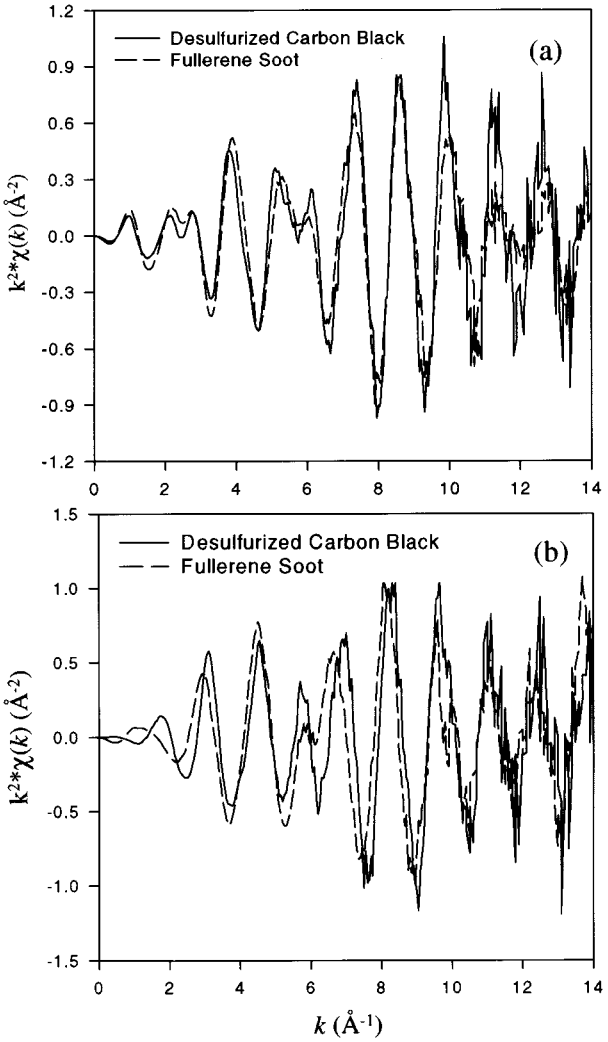

Figure 6. Raw $k^2\chi(k)$ (Å^{-2}) EXAFS data measured at 190 K from carbon-supported [$PtRu_5$]/C nanoparticles after activation at 673 K under H_2 (1atm): (a) Pt L_3 and (b) Ru K edges.

Table 2. Fitting Parameters Obtained by Simultaneously Fitting the Pt L_3 and Ru K Edge EXAFS Data Measured from the [$PtRu_5$]/C Nanoparticles

	carbon black (low-*S*)	fullerene soot
First Nearest Neighbor Distance (Å)		
Pt−Pt	2.69(2)	2.69(1)
Pt−Ru	2.70(1)	2.68(1)
Ru−Ru	2.66(1)	2.68(1)
Coordination Number		
Pt−Pt	1.9(0.9)	5.2(2.0)
Pt−Ru	4.2(0.8)	3.4(1.1)
Ru−Pt	0.8(0.2)	0.7(2)
Ru−Ru	6.0(1.3)	3.5(1.2)
Pt−M	6.1(0.8)	8.6(1.5)
Ru−M	6.8(1.6)	4.2(1.6)
Ru−low-*Z*-atom (C)	0	1.6(3)
Pt−low-*Z*-atom (C)	0	0
Mean Square Disorder (Å^2)		
Pt−Pt	0.0026(36)	0.0061(35)
Pt−Ru	0.0034(13)	0.0034(21)
Ru−Ru	0.0054(13)	0.0048(21)

displayed in Tables 2 and 3 for [$PtRu_5$]/C and [Pt_2Ru_4]/C, respectively (see also Figures 11−14).

The first-shell bond distances determined from the fit are consistent with the values found in the reference materials (Tables 2 and 3). In general, the fitting results for the first-shell coordination numbers (Tables 2 and 3)

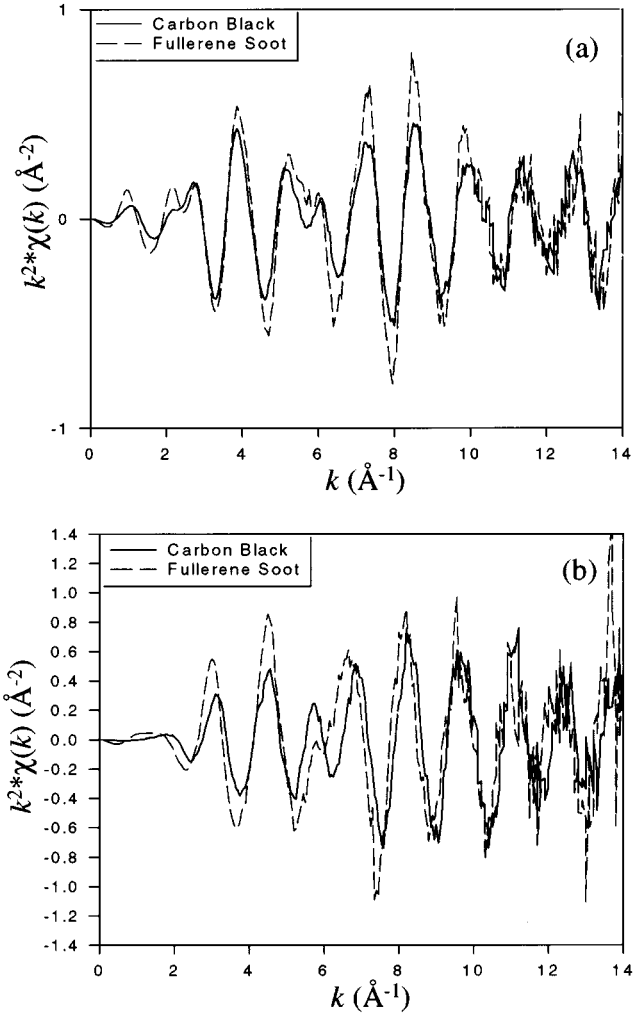

Figure 7. Raw $k^2\chi(k)$ (Å^{-2}) EXAFS data measured at 190 K from carbon-supported [Pt_2Ru_4]/C nanoparticles after activation at 673 K under H_2 (1 atm): (a) Pt L_3 and (b) Ru K edges.

Table 3. Fitting Parameters Obtained by Simultaneously Fitting the Pt L_3 and Ru K Edge EXAFS Data Measured from the [Pt_2Ru_4]/C Nanoparticles

	carbon black	fullerene soot
First Nearest Neighbor Distance (Å)		
Pt−Pt	2.73(1)	2.71(2)
Pt−Ru	2.70(1)	2.69(1)
Ru−Ru	2.66(1)	2.68(1)
Coordination Number		
Pt−Pt	4.4(9)	6.0(1.9)
Pt−Ru	3.3(4)	3.2(1.1)
Ru−Pt	1.7(2)	1.6(6)
Ru−Ru	3.7(4)	4.1(1.7)
Pt−M	7.7(7)	9.2(1.5)
Ru−M	5.4(3)	5.7(1.1)
Ru−low-*Z*-atom (C)	0	1.6(3)
Pt−low-*Z*-atom (C)	0	0
Mean Square Disorder (Å^2)		
Pt−Pt	0.0079(8)	0.0056(25)
Pt−Ru	0.0056(8)	0.0034(20)
Ru−Ru	0.0039(7)	0.0045(25)

reflect the Ru-rich nature of the nanoparticles. The fact that significant Pt−Pt interactions exist demonstrates that the nanoparticles must be obtained from the condensation of several molecules of the precursors ($PtRu_5C(CO)_{16}$ and $Pt_2Ru_4(CO)_{18}$, respectively).

The data also suggest that the structural environments sampled by the Pt and Ru centers in the supported

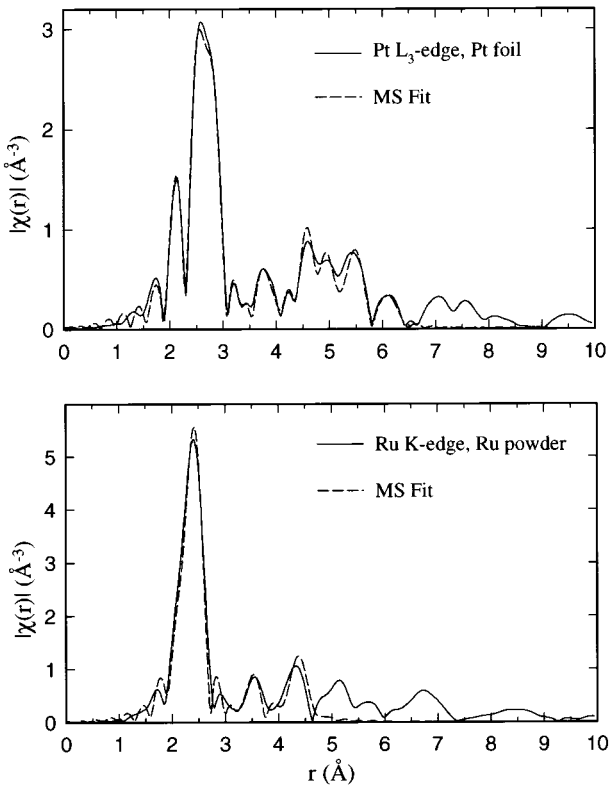

Figure 8. Fourier-transformed EXAFS data measured from the reference materials at 190 K (solid line), and the multiple scattering fit results (dashed line): (a) Pt L_3 edge from a Pt foil (0.05 mm); (b) Ru K edge from Ru powder.

particles are not statistical and, thus, some degree of atomic segregation must occur. The compositional asymmetry in the first-shell coordination environments of Pt and Ru shows a marked preference for homometallic coordination. This fact can be quantified by comparing the statistically predicted ratio of Ru−Pt bonds to Ru−M bonds ($N_{RuPt(1)}/N_{RuM(1)}$) with the value determined by EXAFS. The statistical distribution of metal neighbors around the Ru for the 1:5 composition would result in a $N_{RuPt(1)}/N_{RuM(1)}$ ratio of 0.17, whereas the value determined by EXAFS was 0.17 ± 0.08 for the fullerene soot and 0.12 ± 0.04 for desulfurized carbon black. More strikingly though, the statistical $N_{PtRu(1)}/N_{PtM(1)}$ ratio is 0.83 and the values determined by EXAFS for fullerene-soot-supported and desulfurized carbon black were 0.40 ± 0.15 and 0.62 ± 0.14, respectively. We have previously found for the [$PtRu_5$] nanoparticles on a nascent carbon black support values of 0.12 ± 0.03 and 0.4 ± 0.3 for these two ratios. The trend in the asymmetries is even more evident in the Pt_2Ru_4 clusters. The statistical distribution for the 2:4 composition would result in a $N_{RuPt(1)}/N_{RuM(1)}$ ratio of 0.33, whereas the values determined by EXAFS for carbon black and fullerene soot were 0.31 ± 0.04 and 0.28 ± 0.12, respectively. Again, the more striking result for the 2:4 composition is seen in comparing the statistical $N_{PtRu(1)}/N_{PtM(1)}$ ratio (0.66) and the values determined by EXAFS for carbon black and fullerene soot (0.43 ± 0.06 and 0.35 ± 0.13, respectively). These findings suggest a strong preference for the selection of Pt−Pt and Ru−Ru bonding at the expense of heterometallic bonding in the nanoparticles.

Another finding of note is the effect the support has on the final structure of the nanoparticles. The marked difference between the supports is indicated by the presence, in the EXAFS spectra, of Ru−low-*Z*-atom interactions on the fullerene soot support (Tables 2 and 3). The presence of these interactions leads to an increase in atomic segregation, as seen above, as well as the possible formation of Ru−C compound phases.

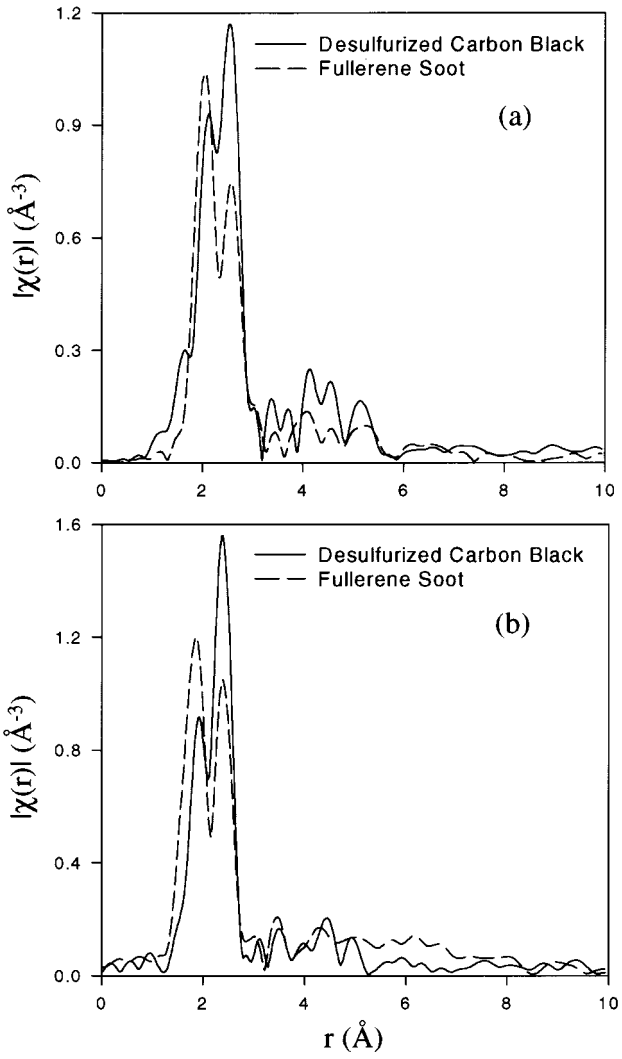

Figure 9. Fourier-transformed EXAFS data measured at 190 K from the carbon-supported [$PtRu_5$]/C nanoparticles after activation at 673 K under H_2: (a) Pt L_3 and (b) Ru K edges.

Characterization of Nanoparticles through XANES. Representative X-ray absorption near edge structure data obtained on the Pt L_3 edge of [$PtRu_5$]/C are shown in Figure 15. The spectra (see ref 6b for an illustration of the representative line shapes) used to calculate these data were measured at different temperatures during the reductive condensation of the nanoparticles. The edge jumps of the supported particles were carefully aligned relative to the inflection point on the absorption edge jump measured simultaneously on the reference metal (Pt foil). The shift between different data sets was defined as the energy difference between the data and the inflection points on the edge jump of the Pt reference. As we have demonstrated previously,[6] choosing Pt metal as a reference has an advantage because the defined shift naturally characterizes the transformation to the final metallic state of the particles. The data clearly demonstrate that the edge energy progressively shifts during the heating cycle toward a limiting value consistent with a metallic state. Table 4 illustrates the final energy shift for each of the supported nanoparticles. In this case, the Pt L_3 edge of the fullerene-soot-supported nanoparticles continues to yield a shift toward higher energies.

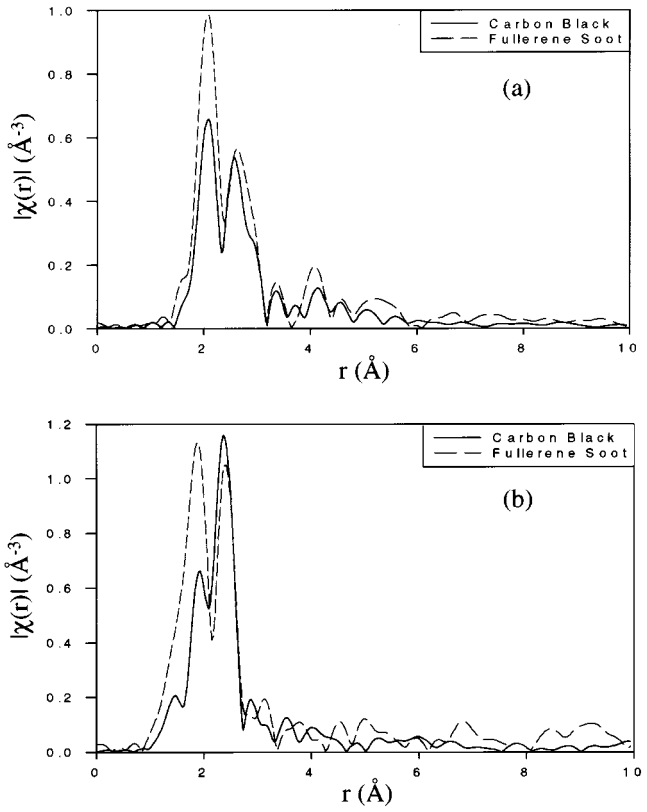

Figure 10. Fourier-transformed EXAFS data measured at 190 K from the carbon-supported $[Pt_2Ru_4]$/C nanoparticles after activation at 673 K under H_2: (a) Pt L_3 and (b) Ru K edges.

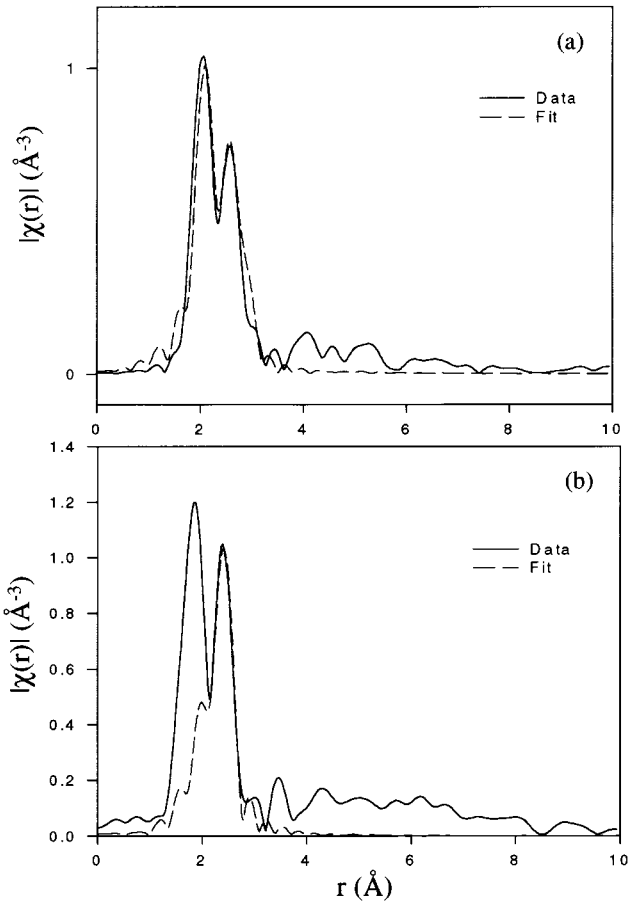

Figure 11. Fourier-transformed EXAFS data measured at 190 K from the $[PtRu_5]$/fullerene soot nanoparticles after activation at 673 K under H_2 (solid line), and the fit results (dashed line): (a) Pt L_3 and (b) Ru K edges.

Discussion

The dispersion and chemical reduction of the $PtRu_5C(CO)_{16}$ and $Pt_2Ru_4(CO)_{18}$ molecular cluster precursors on different carbon supports, namely carbon black, fullerene soot, and desulfurized carbon black, result in the formation of bimetallic nanoparticles with an average particle size distribution between 1.0 and 1.5 nm and a narrow compositional distribution centered on the stoichiometric composition (1:5 for $PtRu_5C(CO)_{16}$ and 2:4 for $Pt_2Ru_4(CO)_{18}$) of the precursors. The most striking result of the study, then, is that the cluster-activation processes appear to be reasonably insensitive to these aspects of chemistry. A somewhat more labile precursor (Pt_2Ru_4, which lacks a carbide core) proved just as effective in giving well-defined nanoparticles as the more robust precursor used to prepare the $[PtRu_5]$/C samples. As we have shown previously, the nanoparticles (for the $PtRu_5$ case) are best modeled as an fcc hemisphere, with the Pt atoms segregating to the surface of the nanoparticles and away from the substrate, maximizing the number of Pt−Pt bonding interactions.[6] In the following discussion, we will show that this model is consistent with the structure adopted for a broader range of cluster-derived Pt/Ru compositions on a variety of carbon supports.

To provide insight into the morphology of the nanoparticles, we used the first-shell coordination numbers determined from the EXAFS data to estimate the average size and composition of the supported nanoparticles.[6] As was previously reported, the average coordination number of $[PtRu_5]$ nanoparticles supported on carbon black, based on a weighted average of the Pt and Ru first-shell coordination number, was 6.3 ± 1.0. This value is considerably lower than the anticipated value of 12 for an fcc structure. When studying the average coordination numbers (Tables 2 and 3), we find average values of 6.4 ± 2 for $[PtRu_5]$ supported on fullerene soot and 6.5 ± 1.0 for $[PtRu_5]$ on desulfurized carbon black. Similarly, for $[Pt_2Ru_4]$/C, we find average coordination numbers of 6.6 ± 1.0 for the carbon black support and 7.5 ± 1.3 for the fullerene soot support. This reduction in first-shell coordination is directly related to the finite size of the nanoparticles, since the fraction of surface sites with lower coordination numbers increases as the particle size decreases.[16] As we have shown previously, an average coordination number of 6.3 corresponds to an average hemispherical particle diameter of 1.2 nm.[6] It is important to note that this value is close to those inferred from scanning transmission electron microscopy.

Heterometallic bonding interactions are strongly evidenced in the EXAFS data and provide evidence for the formation of bimetallic particles. The EDX compositional data confirm the presence of bimetallic particles. Perhaps more intriguing, though, is the fact that the compositional analyses of discrete particles (Table 1) are indistinguishable from that of the precursors (to within the narrow limits of experimental error).

Having established the size and compositional distributions of these nanoparticles, it is possible to use the relative coordination numbers for the two metals by EXAFS to construct a more detailed model of the average nanoparticle microstructure. As we have described above, the first-shell metal coordination numbers indicate that

(16) (a) Benfield, R. E. *J. Chem. Soc., Faraday Trans.* **1992**, *88*, 1107. (b) van Zon, J. B.; Koningsberger, D. C.; van't Blik, H. F. J.; Sayers, D. E. *J. Chem. Phys.* **1985**, *82*, 5742. (c) Gallezot, P.; Bienenstock, A. I.; Boudart, M. *Nouv. J. Chim.* **1978**, *2*, 263.

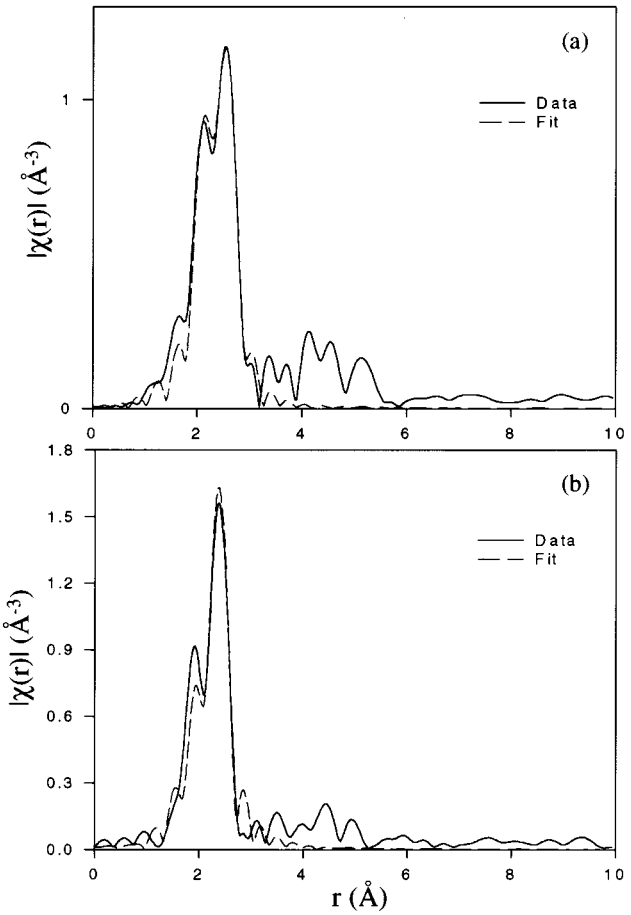

Figure 12. Fourier-transformed EXAFS data measured at 190 K from the [$PtRu_5$]/desulfurized carbon black nanoparticles after activation at 673 K under H_2 (solid line), and the fit results (dashed line): (a) Pt L_3 and (b) Ru K edges.

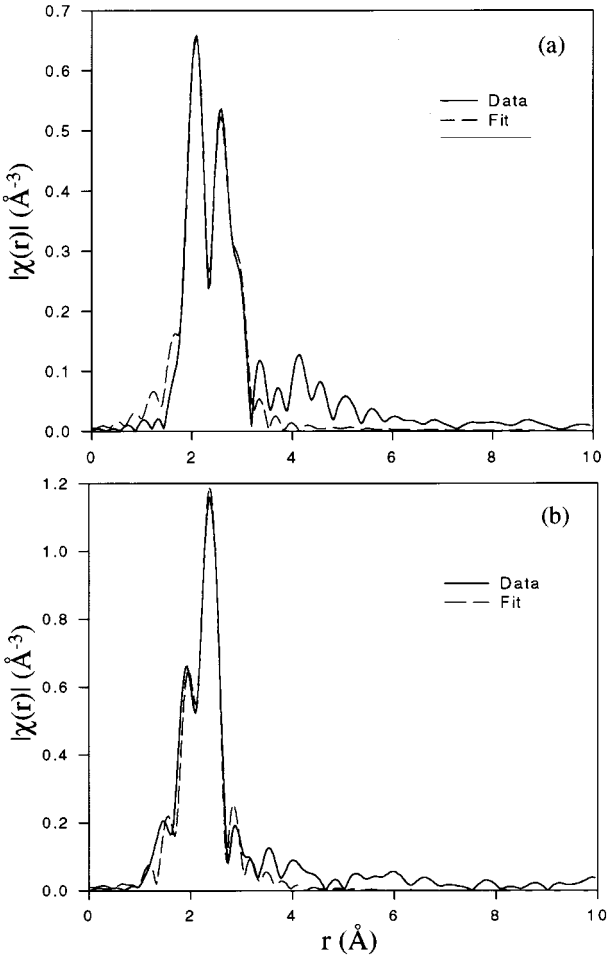

Figure 13. Fourier-transformed EXAFS data measured at 190 K from the [Pt_2Ru_4]/carbon black nanoparticles after activation at 673 K under H_2 (solid line), and the fit results (dashed line): (a) Pt L_3 and (b) Ru K edges.

both Pt and Ru favor nonstatistical homometallic interactions. This suggests that a segregation of the Pt and Ru to nonstatistical environments, ones which are rich in one of each of the respective metals, occurs in the nanoparticle samples. Because the size and compositional distributions are narrow, this segregation cannot arise from the formation of discrete single element clusters of Pt and Ru. The differences observed in the average Pt and Ru coordination environments must arise from an inherent variation in the intraparticle distribution of the metals, since the EXAFS data reflect an average environment in a nearly homogeneous (in size and composition) population of particles. Intraparticle segregation can only result from the partitioning of Pt toward the interior or the surface of the particle. Given the size of the particles, this small number of Pt atoms (~6−12) could easily reside in strictly interior sites, resulting in a Pt first-shell coordination close to 12. The first-shell Pt−M(1) coordination environments shown above do not support this model. We have shown previously that the Pt coordination environment supports a structural model based on a preference for the segregation of Pt to the surface of the nanoparticles.[6] Such segregation effects have been previously described by other investigators.[1,2b−e,3,17] For example, Sinfelt et al. found significant nonrandom distributions in bimetallic systems and attributed it to the formation of raftlike structures in which there is preferential surface segregation.[1a] The presence of Pt surface segregation also has a precedent in bulk $Pt_xRu_{(1-x)}$ alloy phases. For example, Ross et al. found a >90% surface enrichment of Pt in bulk alloys with low Pt compositions (~9 atom %).[18]

Support Effects. Perhaps even more intriguing than the above-noted segregation effects are the differences seen in the nanoparticle structures which originate in the interactions occurring with the different types of carbon support. In the following discussion, we propose a possible model for the differences in behavior seen between nanoparticles supported on fullerene soot and those supported on carbon black (Vulcan XC-72 and desulfurized Vulcan XC-72).

As is evidenced in the EXAFS fitting data (Tables 2 and 3), fullerene-soot-supported nanoparticles show a presence of Ru−low-*Z*-atom (i.e., carbon or oxygen) interactions which are large compared to the experimental uncertainty. While metal−carbon interactions are clearly present in all the particle systems, our earlier studies have suggested that they are highly disordered and thus contribute little magnitude to the EXAFS signal. Clearly different results are obtained on the fullerene soot support phase. Heating the molecular precursors in H_2 results in a reductive condensation during which the carbon-supported molecular precursors lose the carbon monoxide ligand shell.[6b] The desorption of carbon monoxide must occur via an

(17) (a) Miura, H.; Gonzalez, R. G. *J. Phys. Chem.* **1982**, *86*, 1577. (b) Alerasool, S.; Gonzalez, R. D. *J. Catal.* **1990**, *124*, 204. (c) Radmilovic, V.; Gasteiger, H. A.; Ross, P. N. *J. Catal.* **1995**, *154*, 98.

(18) Gasteiger, H. A.; Ross, P. N.; Cairns, E. J. *J. Surf. Sci.* **1993**, *293*, 67.

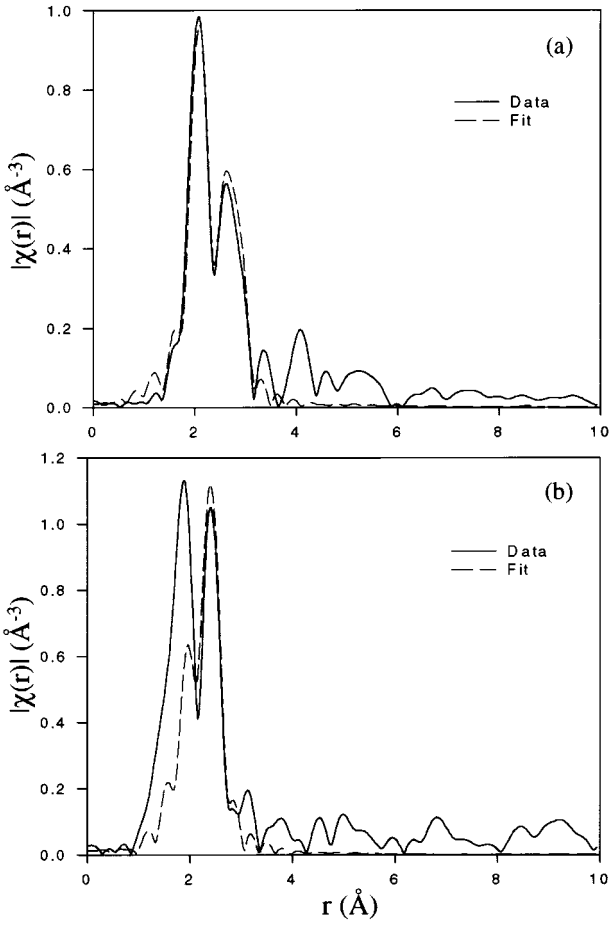

Figure 14. Fourier-transformed EXAFS data measured at 190 K from the $[Pt_2Ru_4]$/fullerene soot nanoparticles after activation at 673 K under H_2 (solid line), and the fit results (dashed line): (a) Pt L_3 and (b) Ru K edges.

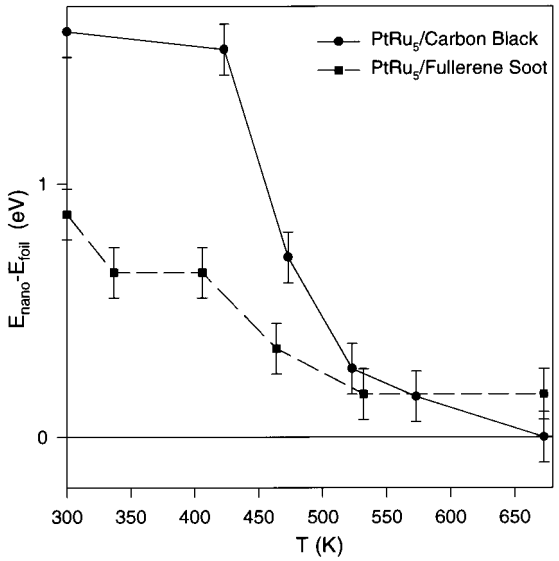

Figure 15. Shift (relative to the Pt metal foil) of the binding energy in the Pt−Ru nanoparticles during their evolution to the metallic state, as measured from XANES.

exchange with bonds to hydrogen, the carbon support, or metal atoms from other molecular precursor clusters. During this condensation process, the Ru must be interacting with (in addition to metal centers) either carbon monoxide, which has not completely desorbed, or low-*Z* atoms provided by the support. Such contributions might be invoked to explain the data seen on the fullerene soot samples. It is therefore necessary to look more closely at the details of the spectroscopy to gain a clearer understanding of the final nanoparticle structures.

Table 4. Energy Shifts Deduced from XANES Spectra after 1 h at 673 K in an H_2 Flow

supported nanoparticle	$E_{nano} - E_{foil}$ (eV)
$[PtRu_5]$/carbon black	0 ± 0.1
$[PtRu_5]$/fullerene soot	0.17 ± 0.1
$[PtRu_5]$/desulfurized carbon black	0 ± 0.1
$[Pt_2Ru_4]$/carbon black	0 ± 0.1
$[Pt_2Ru_4]$/fullerene soot	0.15 ± 0.1

In general terms, then, we see the following structural outcomes. Both $PtRu_5$ and Pt_2Ru_4 cluster precursors give a uniform population of carbon-supported alloy nanoparticles, albeit differing in stoichiometry, as expected from the initial compositions. The final states reached on carbon black supports are consistent with the properties of a metallic ensemble of atoms. Surface segregation of Pt is seen in both the $PtRu_5$ and Pt_2Ru_4 systems. The structures of the particles formed on carbon black are not sensitive to the heteroatom content of the support, suggesting these interactions do not exert a dominating influence over the activated processes involved in the nanoparticle nucleation and growth. The M−C interactions present on these supports are highly disordered.

The properties and structural habits seen in nanoparticles formed on a fullerene soot support, however, are very different in several significant ways. The most notable of those is the electronic structure of the cluster as deduced from the XANES data. These data also provide significant insight into the final state properties, and hence the electronic structure, of the supported nanoclusters. The absorption-threshold resonance observed at the Pt L_3 edge results from the excitation of $2p_{3/2}$ core level electrons into unoccupied 5d states.[19] This resonance intensity is affected by changes in the oxidation state of the absorber. However, more subtle effects, such as dispersion, or changes in the interaction with the support are also important. The edge position, which is, in large part, related to the binding energy of the Pt $2p_{3/2}$ electrons, will be affected by changes in the valence electronic structure and changes in the extraatomic relaxation (i.e., final state effects).[20] As we reported earlier, most of the changes involved in the particle growth, including the maximum desorption rate of the coordinating CO ligand shell, occur in the temperature range 423−473 K.[6b] Our studies suggest that the disruption of the cluster framework above 423 K leads to the loss of CO ligands with a likely substitution of metal−metal (and perhaps metal−hydrogen or metal−support) bonds. This progressive evolution of the bonding environments around the metal cores underlies the edge shifts seen in the XANES data (Figure 15, Table 4). We notice, however, that the final state of the nanoparticles supported on the fullerene soot never reaches a limiting "metallic" state, showing a slight edge shift to higher energies. As mentioned previously, this slight shift could be induced by incomplete reduction or by changes in the valence electronic structure or result from final state effects.[20]

Examining the metal shell structure around the Pt and Ru atoms provides further evidence as to the nature of the final nanoparticle structure seen in these latter samples. The presence of a substitutional Pt−Pt bonding contribution indicates that the nanoparticles include metal atoms from more than one precursor molecule. We have

(19) (a) Lytle, F. W. *J. Catal.* **1976**, *43*, 376. (b) Mansour, A. N.; Cook, J. W.; Sayers, D. E. *J. Phys. Chem.* **1984**, *88*, 2330. (c) Meitzner, G.; Via, G. H.; Lytle, F. W.; Sinfelt, J. H. *J. Phys. Chem.* **1992**, *96*, 496.

(20) Citrin, P. H.; Wertheim, G. K. *Phys. Rev. B* **1983**, *27*, 317.

previously shown that the Pt and Ru homometallic bond distances are indicative of the level of alloying in the nanoparticles.[6b] Specifically, the splitting between the Pt−Pt, Pt−Ru, and Ru−Ru bond distances should be smaller for a well-alloyed material compared to the splitting of the corresponding distances in the original precursor molecules, where this splitting was large (Pt−Ru and Ru−Ru distance ranges are 2.91(8) and 2.88(6) Å for $PtRu_5C(CO)_{16}$ and 2.77(7) and 2.96(8) Å for $Pt_2Ru_4(CO)_{18}$).[10] The Pt−Pt, Pt−Ru, and Ru−Ru bond distances obtained for $PtRu_5$ supported on fullerene soot were 2.69(1), 2.68(1), and 2.68(1) Å, respectively (Table 2). We previously reported values for $PtRu_5$ on nascent carbon black of 2.69(3), 2.70(1), and 2.70(1) Å, respectively.[6a] The values for the Pt−Pt and Ru−Ru bond distances for Pt_2Ru_4 supported on nascent carbon black are 2.73(1), 2.70(1), and 2.66(1) Å, respectively, while those for the fullerene-soot-supported material are 2.71(2), 2.69(1), and 2.68(1) Å, respectively (Table 3). These results show that, for both supports, metallic bond distances are much closer to each other in the nanoparticles than in their respective precursors (to within experimental error). As we have previously reported, this fact is consistent with reduced nanoparticles.[6b]

This conclusion is also strongly supported by the average metal coordination numbers measured in the EXAFS (see above) and the STEM data, both of which support a structural model based on an fcc hemispherical cuboctahedron.[6] Other factors thus must be involved to explain the low-*Z*-atom (presumably carbon) interactions seen for the fullerene-soot-supported samples.

There are two possible models for the interactions occurring with the surface. The first suggests that a possible higher symmetry of the fullerene soot support leads to differences in the disorder characterizing its interactions with the nanoparticles; the second, more plausible explanation is the formation of a Ru-carbide phase. The edge shift and change in electronic properties of the nanoparticle more strongly support the latter model. Other than these changes in the electronic structure, we know little about the detailed structure of this carbide phase except to note that the average number of Ru−C interactions seen and the detailed metal shell structure are inconsistent with the formation of a bulk phase. This suggests that reactions between the nanoparticle and the support may only be occurring at the contact boundaries. A structural model for this interaction may be the Ru_3 cluster face coordination to C_{60} exhibited by the complexes $Ru_3(CO)_9(\mu^3\text{-}\eta^2,\eta^2,\eta^2\text{-}C_{60})$,[21a] $Ru_5C(CO)_{11}(PPh_3)(\mu^3\text{-}\eta^2,\eta^2,\eta^2\text{-}C_{60})$,[21b] and $Ru_5C(CO)_{11}Pt(dppe)(\mu^3\text{-}\eta^2,\eta^2,\eta^2\text{-}C_{60})$,[21c] although these molecules as such represent better models for intermediates in the activation process for the final nanoparticles.

Conclusion

Bimetallic nanoparticles supported on various carbon supports, including carbon black, fullerene soot, and desulfurized carbon black, were prepared from $PtRu_5C(CO)_{16}$ and $Pt_2Ru_4(CO)_{18}$ molecular precursors by activation in H_2 at 673 K. The EXAFS data indicated that these nanoparticles behaved similarly to those reported previously.[6] Differences in the coordination environments of the two metals reflect the preferential occupation of surface sites by the Pt centers. In support of the spectroscopic measurements, microscopy demonstrated the formation of an extremely narrow size distribution in the particles. The compositional distribution, which was found to be 1:5 for $[PtRu_5]$ and 2:4 for $[Pt_2Ru_4]$, suggests a uniform coalescence of precursor clusters during activation. The nanoparticle interaction with the fullerene soot suggests formation of a Ru carbide phase at the support−nanoparticle boundary.

Acknowledgment. This work was supported by the Defense Advanced Research Project Agency through the Office of Naval Research (Grant N00014-96-1-0490) and the Department of Energy through the Seitz Materials Research Laboratory (Grant DEFG02-91-ER45439). We thank Dr. Kwangyeol Lee for the preparation of $PtRu_5C(CO)_{16}$ and $Pt_2Ru_4(CO)_{18}$.

LA980921B

(21) (a) Hsu, H. F.; Shapley, J. R. *J. Am. Chem. Soc.* **1996**, *118*, 9192. (b) Lee, K.; Hsu, H. F.; Shapley, J. R. *Organometallics* **1997**, *16*, 3876. (c) Lee, K.; Shapley, J. R. *Organometallics* **1998**, *17*, 3020.